







Towards Polymer-Free, Femto-Second Laser-Welded Glass/Glass Solar Modules

David L. Young , Member, IEEE, Timothy J. Silverman , Nicholas P. Irvin , Daniel Huerta-Murillo , Bill Holtkamp , and Nick Bosco 

Abstract—This article explores the use of femtosecond (fs) lasers to form glass-to-glass welds for hermetically sealed, polymer-free solar modules. Low-iron solar glass coupons were welded together without the use of glass filler using a fs laser with dedicated optics to elongate the focal plane parallel to the incident beam. The resulting welds were then stress tested to failure to reveal the critical stress intensity factor, K_{Ic} . These values were used in a structural mechanics model of a $1\text{ m} \times 2\text{ m}$ glass/glass module under a simulated static load test. The results show that the fs laser welds are strong enough for a suitably framed module to pass the IEC 61215 static load test with a load of 5400 Pa. Key to this finding is that the module must be framed and braced, and the glass must be ribbed to allow pockets for the cells and welds inside the border of the module. The result is a module design that is completely polymer free, hermetically sealed, has improved thermal properties, and is easily recycled.

Index Terms—Lasers, mechanical stress, solar panels, welding.

I. INTRODUCTION

MANY solar module degradation mechanisms are tied directly to the use of polymers in the laminated stack [2]. These failures include discoloration, which decreases photon flux to the cells, and delamination that can lead to moisture and oxygen in-diffusion, enabling contact corrosion. Even with no delamination or cracks, polymers are poor barriers to moisture and oxygen compared with glass. Perovskite cells are extremely sensitive to moisture and oxygen and will likely need a nonpolymer-based encapsulant to avoid severe degradation at the module level. This contribution explores a new module design that eliminates polymer materials and instead forms a glass/glass-welded hermetically sealed module using femtosecond (fs) laser technology.

Encapsulant between the glass has been omitted in the “NICE” module by Apollon Solar [3] and in work done by

Barth et al. [4] from Colorado State University, where only a polyisobutylene (PIB) polymer edge seal was used to join the glass/glass module. However, even the best double-pane architectural windows held together by PIB have seal failure after 20–30 years [5], [6]. Eliminating ethylene vinyl acetate (EVA) (or any polymer) from the module greatly reduces the chances for degradation, including delamination, corrosion, discoloration, and potential-induced degradation, all related to moisture or ion ingress interacting with encapsulants [7], [8]. The elimination of EVA within the module can also improve the optics of the module [9].

Edge sealing by laser *glass/frit* sealing is known [10], [11], [12] and has been tested on soda-lime photovoltaic (PV) glass [11]. However, these welds are brittle and not strong enough for outdoor module designs. Key to this present work is the use of a relatively new glass welding regime using fs pulsed lasers, which allows a strain-free, high-strength, hermetic seal using the nonlinear absorption of laser photons to produce localized heating at the glass/glass interface [13], [14], [15]. Miyamoto et al. [16] illustrated these material science concepts well. For IR continuous wave or nanosecond (ns) lasers, the light is absorbed at the surface of the glass (weld), but the free surface allows shrinkage stress to generate cracks in the glass during cool down leaving the weld region under tensile stress. This type of welding is only appropriate for glass with a low coefficient of thermal expansion, such as quartz. However, if fs pulses are used, the more intense photon flux allows nonlinear absorption of the energy at the focal point near the *interface* of the two glass surfaces. This allows a stress-free weld to be formed without a free surface because the isotropic pressure on the molten glass does not allow the glass to plastically deform. Thus, the use of fs lasers for stress-free welds is vital to forming strong, durable welds and is the key differentiator from the previous work.

Here, we present a preliminary proof-of-concept study on using glass/glass fs laser welding without filler to seal glass/glass photovoltaic modules. Our study involves forming fs laser welds between two solar glass pieces and performing a controlled break of the weld to measure the critical stress intensity factor of the weld. Next, we perform a structural mechanics study of a simulated laser-welded, glass/glass module under static load conditions. The model measured the stress intensity factors over the area of a $1\text{ m} \times 2\text{ m}$ module. We found that, with a slight redesign of the module (embossed glass features, bracing of the glass), the stress intensity factors at the weld lines do not exceed the measured critical stress

Manuscript received 29 September 2023; revised 13 November 2023 and 31 January 2024; accepted 5 February 2024. Date of publication 21 February 2024; date of current version 19 April 2024. This work was supported in part by the National Renewable Energy Laboratory (NREL), operated by Alliance for Sustainable Energy, LLC, for the U.S. Department of Energy (DOE) under Contract DE-AC36-08GO28308 and in part by DuraMat Consortium under SPARK Program. (Corresponding author: David L. Young.)

David L. Young, Timothy J. Silverman, Nicholas P. Irvin, and Nick Bosco are with National Renewable Energy Laboratory, Golden, CO 80401 USA (e-mail: david.young@nrel.gov).

Daniel Huerta-Murillo and Bill Holtkamp are with TRUMPF Inc., Santa Clara, CA 95054 USA.

Color versions of one or more figures in this article are available at <https://doi.org/10.1109/JPHOTOV.2024.3364823>.

Digital Object Identifier 10.1109/JPHOTOV.2024.3364823

U.S. Government work not protected by U.S. copyright.

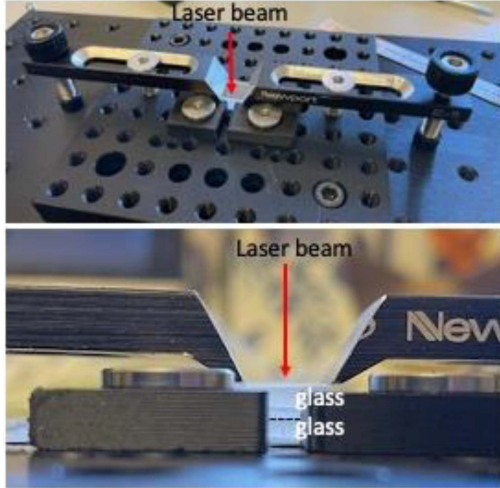


Fig. 1. Image of jig used to press two pieces of glass together during the laser welding process.

intensity factor even under the maximum load of 5400 Pa. Finally, thermal–optical analysis of the laser-welded module indicates that its operational temperature will be within a couple of degrees of that of a conventionally encapsulated module if the gas cavity in the laser-welded module is kept under $250\ \mu\text{m}$ in thickness, with thermal benefits seen for air gaps under $100\ \mu\text{m}$.

II. EXPERIMENT: GLASS/GLASS FS LASER WELDING

Low-iron, nontextured solar glass samples of 3 mm thick were cut to $10\ \text{mm} \times 12\ \text{mm}$ and the edges were ground to remove edge cracks. The samples were cleaned and mounted onto an optical bench using a jig to press two samples together, as shown in Fig. 1. The glass pieces were pressed together under hand-tight torque from the screws, as shown in Fig. 1. A 20 W fs laser (TruMicro 2030 – TRUMPF Lasers) of wavelength 1030 nm equipped with TOPWELD optics was used to weld the glass pieces together. Five to six laser weld lines were formed parallel to the long edge of the glass separated by $70\text{--}200\ \mu\text{m}$, as shown in Fig. 2(a). Laser power was varied between 12.0% and 13.5% of the maximum based on visual weld quality.

III. EXPERIMENT: CRITICAL STRESS INTENSITY FACTOR, K_{Ic}

Welded samples were glued to metal cylinders on the flat sides of the glass samples, as shown in Fig. 3 (left). These cylinders were attached to a mechanical force test stand that applied a tensile force perpendicular to the weld lines, as shown in Fig. 3 (right). The test measured the maximum force needed to break the weld lines and separate the two glass samples. Equation (1) was used to calculate K_{Ic} of the weld

$$K_{Ic} = \sigma \sqrt{\pi a} F(a/b) \quad (1)$$

where

$$F(a/b) = \frac{1.122 - 0.561(a/b) - 0.015(a/b)^2 + 0.091(a/b)^3}{\sqrt{1 - a/b}} \quad (2)$$

σ is the remote stress on the weld and a and b are the geometric lengths, as defined in Fig. 2(b). The function $F(a/b)$ is defined

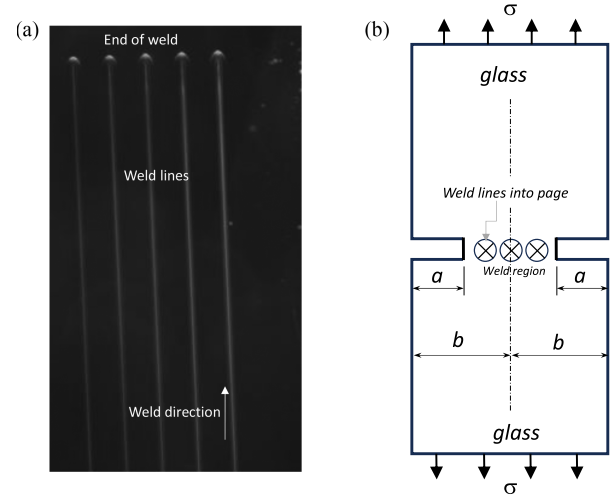


Fig. 2. (a) Optical image of laser weld lines between two glass samples. (b) Geometric variables used in (1) and (2) (Figure modified from [1]).

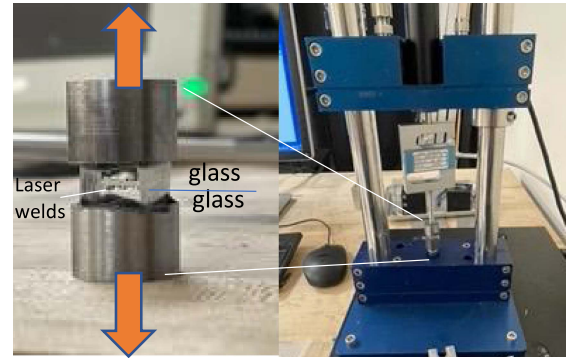


Fig. 3. Glass/glass laser-welded sample glued to two metal cylinders for K_{Ic} measurement (left). Press to measure tensile force to weld breakage (right).

in [17] and ranges from 2.1 to 3.4 for our samples. Fig. 4 is a graph of the measured K_{Ic} values for different weld parameters (number of weld lines, spacing between weld lines, and percent of total laser power). The two dashed horizontal lines on the graph show the range of K_{Ic} values for typical soda-lime float glass [18]. The graph indicates that laser power plays a major role in how tough the glass/glass weld can be. For our limited number of samples, the higher 13.5% laser power gave higher values than most of the lower power welds. However, the number of weld lines and the spacing between the lines seem to also play a smaller role in determining the K_{Ic} value. More work is needed to optimize the weld parameters, but the data in Fig. 4 are encouraging in which some of the welds are near the K_{Ic} values of homogeneous glass.

IV. MODELING: FULL-SIZED GLASS-WELDED MODULE

To place the measured K_{Ic} values in context to a laser-welded module, we developed a structural mechanics model of a $1\ \text{m} \times 2\ \text{m}$ glass/glass laser-welded module in COMSOL. The module contained no polymer laminate materials between the glass sheets. In order to make space for a typical silicon cell and the associated interconnects, we assumed that the glass sheets were made by a rolling process with embossed indentations (see

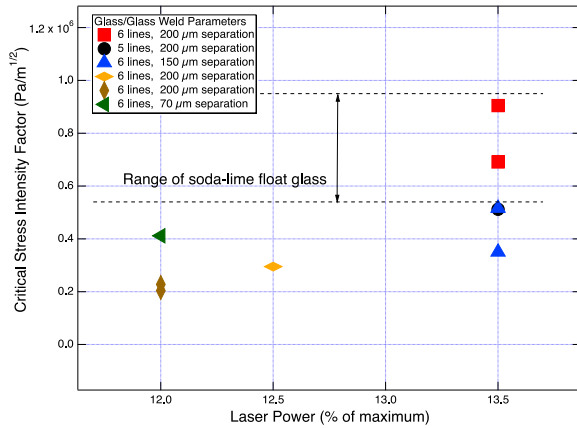


Fig. 4. Measured K_{IC} values for welds made with different laser powers, number of weld lines, and spacing between the weld lines. The horizontal lines show the range of K_{IC} values for typical soda-lime float glass.

schematics in Fig. 5). These indentations are approximately 550 μm deep to provide space for the thickness of the wafer ($\sim 130\text{--}150\ \mu\text{m}$) plus multibusbar wires ($\sim 200\ \mu\text{m}$ thick) on both sides of the cell. This embossed depth is consistent with allowable embossed aspect ratio features of less than 20% of the thickness of the 3 mm glass [19]. If 2-mm-thick glass is used, then a 275 μm deep indentation would need to be embossed in both the top and bottom glass sheets to accommodate the cell plus busbar wires. The model allowed us to vary the embossed features, which included “ribs” in the glass parallel to the long edge of the module. Fig. 5(a) shows a schematic of the embossed glass with cavities for the cells, and flat regions on the edges and on top of the ribs that allow the two sheets of glass to touch for laser welding.

As with most large modules, a frame and two cross braces are needed to minimize the amount of deflection in the module. We modeled an extruded aluminum L-shaped frame with a small box section and cross braces with a box cross section directly supporting the glass sheets. The frame and cross braces are attached to the glass module with a thin layer of silicone and the frame is constrained for out-of-plane displacement at the module mounting points, roughly a quarter of the module’s total length from its ends (see Fig. 5(b)).

The model then simulated a uniform static load over the surface of the module and calculated the out-of-plane displacement of the module and the driving force for weld cracking, J-integral, at an intentionally placed flaw along the weld direction (see Fig. 5(b)). Considering glass is a linear elastic material

$$J = \frac{K_I^2}{E'} + \frac{K_{II}^2}{E'} + \frac{K_{III}^2}{2\mu}$$

where K_I , K_{II} , and K_{III} are the three modes of crack opening, E' denotes the plane strain Young’s modulus, and μ is the shear modulus.

Since K_I is the most pertinent mode to crack propagation in glass, it is, therefore, considered conservatively as the only contribution in this analysis [20].

The heat map in Fig. 5(b) shows the calculated deflection of the glass/glass module in the static load test of IEC 61215, at

a test load of 5400 Pa [21]. The calculated K_I values evaluated at the inner interface of the outermost sealing welds running lengthwise (top graph) and widthwise (right graph) are presented in Fig. 5(b) and represent the region of highest driving force for cracks in the welds under simulated static load conditions. These plots show, for three different loads, that the K_I values are near zero on the edges, rise and then fall to the point under the frame brace and mounting location (arrows in Fig. 5(b)) and then rise to their maximum at the center of the module. The K_I values are symmetric from 0–1 m to 1–2 m. The same type of information for the width of the module is shown in the right graph, but, here, the K_I values are much lower and are periodic between the edge of the module and at each welded rib. For reference, we plot the average K_{IC} value of glass and the average K_{IC} value of the best two laser weld results from this study on the two graphs.

V. DISCUSSION

The main takeaway from the graphs in Fig. 5 is that the K_I of the glass under the three loads is less than the K_{IC} of the glass/glass fs laser welds. This implies that the fs laser-welded glass/glass module with a suitably stiff frame will survive the IEC 61215 5400 Pa static load test. The multiple welded ribs running lengthwise help to limit the deflection and, hence, the K_I in the right graph (well below K_{IC} of glass and the laser welds), but the top graph shows that welded widthwise ribs and/or stiffer support should be used to increase the safety factor of this module design.

This preliminary study showed that glass/glass fs laser welding is tough enough to withstand the stress in a solar module under static load testing, provided that adequate framing and bracing are provided in the mounting structure. Optimization of the laser welding parameters and embossed glass features should be done before load tests are either further simulated or experimentally measured. However, given the nature of the glass/glass welds, the module should be made as stiff as possible to avoid excessive displacement under load.

The excellent measured K_{IC} values of the laser welds indicate that the gap between glass samples during welding was smaller than 10 μm as this is the known maximum gap to support glass/glass welding [22]. This observation is also consistent with the typical micron-scale roughness of nontextured rolled glass used for this experiment and in modules [19].

This study was designed to only test the K_{IC} of fs laser welds on solar glass and to simulate a module static load test to see if the welds were tough enough to survive. We may conclude that they are. Moving forward, we briefly address three other concerns for the new all glass modules:

- 1) electrical feedthroughs;
- 2) scaling the welding process to industrial lines;
- 3) heating effects of a glass/glass, polymer-free module.

Electrical feedthroughs are a vital part of any module design because they provide electrical access to the semiconductor device to the outside circuit while preventing the exchange of the atmosphere into the module. Typical modules use polymers to seal electrical feedthroughs, but our goal is to remove polymers from the module and provide a hermetically sealed product. fs

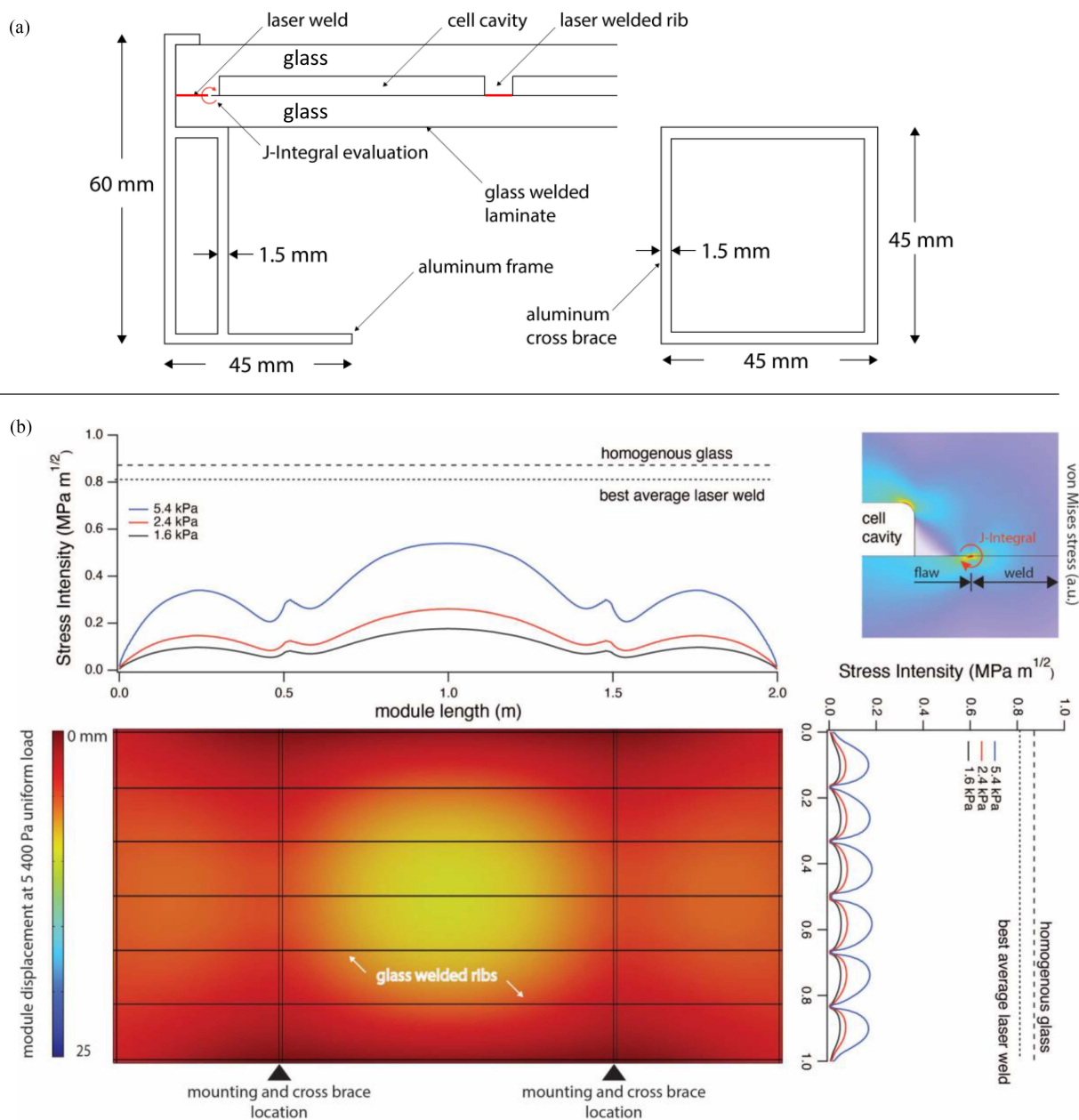


Fig. 5. Structural mechanics modeling results of a laser-welded glass/glass module framed and supported with two crossbar braces [(a) and arrows in (b)] under 5400 Pa of uniform static load. The heat map shows the displacement of the module glass sheets (middle). The 2-D schematic of the edge sealing weld orientation, flaw, and J-integral path (top right). The 1-D plots of the driving force for weld cracking along the edges (top) and ends (right) of the module. The two straight lines in these plots denote the average K_{IC} for homogenous glass and the best average measured laser welds from this study.

laser welding enables hermetically sealed glass-to-metal welds [23] and has been demonstrated as a fabrication path to fuse glass protective endcaps onto metal sleeves for optical fibers [16]. Glass-to-titanium welds have been qualified for medical implant devices [24], but thermal expansion mismatch between most metals and glass will likely cause cracking during the thermal cycling of outdoor PV modules. However, metal alloys, such as Kovar and Invar [25], with matched thermal expansion coefficients to glass, may provide a route to develop a rugged glass-to-metal hermetically sealed feedthrough for PV modules. Existence proof for this idea is well known in the scientific vacuum industry where hot-cathode ion gauges have metal/glass

feedthroughs with allowable bakeout temperatures exceeding 400 °C [26].

Fig. 6 shows a concept schematic for an industrial tool to laser weld solar modules. The tool has a single laser that powers multiple laser weld heads mounted over the glass/glass module. The glass sheets are moved under the heads between 10 and 50 mm/s and are pressed together by top and bottom rollers to ensure a gap of $< 3 \mu\text{m}$ between the sheets. In Fig. 6, an optical sensor [27] is used to monitor the gap and the z -axis of the glass/glass interface to provide real-time feedback adjustment to the focal plane of the lasers. This will account for natural variations in the glass thickness and provide feedback on weld

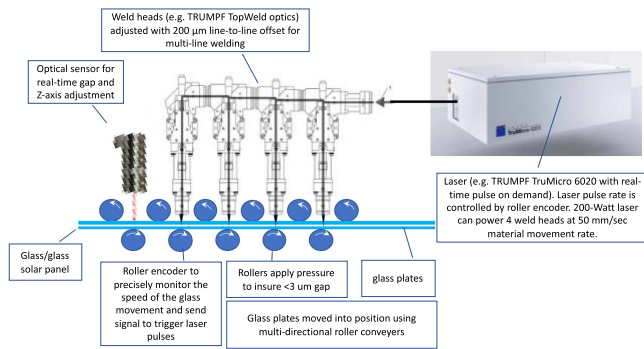


Fig. 6. Schematic concept drawing of large area fs laser welding system for solar modules.

quality. Using this tool as a proxy for an industrial fs laser welding system, we can make some rough comparisons to the traditional lamination process to estimate if the welding process is feasible for high-throughput, low-cost module manufacturing. **Heating:** For traditional lamination, the entire module needs to be heated to about 135 °C and held there for the laminate to cure and then cool to room temperature. For the fs laser welding process, only local heating at the weld site is needed while the rest of the module (within a few mm of the weld) remains at room temperature. **Throughput:** A typical lamination process requires pressing and curing times of approximately 15–21 min. The laser welding tool, as illustrated in Fig. 6, has a maximum weld speed of 5 cm/s, which translates to 5.3 min to weld the module design, as shown in Fig. 5. **Cost:** A small 1 m × 2 m laminator costs about \$70 000, uses 2–3 laminate layers per module, and consumes about 27 kW while operating [28]. A tool of this size would have a throughput of one module every 20 min. Larger laminators exist and may have better economies of scale [29]. The laser welding tool, as shown in Fig. 6, is estimated to cost about \$550 000, has no material inputs, uses about 7 kW in operation, and can weld about four modules in 21 min.

Finally, the removal of polymer laminates from a PV module may have beneficial thermal effects that could translate to decreased power degradation rates and reductions in levelized cost of electricity (LCOE) if the gas cavity that replaces the laminate encapsulant is kept below approximately 100 μm in thickness. Encapsulants, such as EVA, absorb infrared light within silicon modules [30], [31]. Thus, the elimination of absorption that occurs in encapsulants would yield reduced heat generation and module temperatures [32]. In addition to lower heat generation, the switch from an encapsulant to a gas cavity would also change the thermal resistance between the photovoltaic cell and the front module glass. That change can either reduce or increase the temperature of the cell material depending on whether the thermal resistance of the gas cavity is greater or smaller than that of the encapsulant layer. The combined impact of the module absorption and thermal resistance is considered by applying the heat-flow framework of Hammami et al. [33] to the optical-thermal model of Irvin et al. [32], numerically solving a system of equations among the cell, front glass, and rear glass temperatures.

The temperature of the cell within a laser-welded module depends critically on the thickness of the gas cavity, as shown

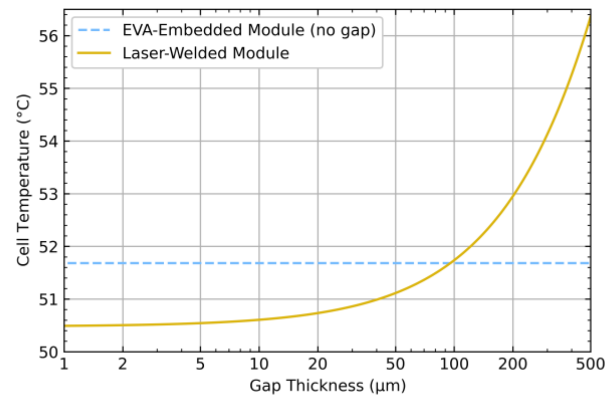


Fig. 7. Thermal impact of an air cavity on the temperature of a laser-welded glass/glass module. The horizontal line shows the temperature of a conventional module encapsulated with an EVA instead of an air gap. The removal of EVA yields lower temperatures if the air gap is kept below approximately 100 μm.

in Fig. 7. These simulations were done for a selective-emitter passivated emitter rear contact cell (PERC) cell with a 24% efficiency under 1 sun, 25 °C ambient, 1 m/s wind speed, and open-rack conditions. The module architecture is glass/glass with symmetric air gaps between the cell and the front and rear glass. The thermal conductivity is taken as 0.028 W m⁻¹ K⁻¹ for air compared with 0.23 W m⁻¹ K⁻¹ for EVA. Further modeling assumptions are detailed in [32]. It is seen that the laser-welded module has a thermal advantage or disadvantage depending on the gap thickness. For a gap thickness of 5 μm or less, the cell temperature within the laser-welded module is 1.2 °C lower than that of a corresponding EVA-embedded module, a change due equally to the removal of absorption and thermal resistance across the EVA layer. At around 100 μm of gap thickness, the net temperature difference becomes zero as the increase in thermal resistance negates the impact of reduced heat generation in the module. The cell temperature increases at thicker air gaps, leading to a 1.3 °C higher temperature than the EVA-embedded module for an air gap thickness of a 200 μm. While 200 μm has been shown to be an optimal diameter for wires in multiwire busbar configurations based on the consideration of shading and electrical resistance alone, thinner wire diameters offer lower cell breakage, altogether implying that the practical gap thickness for a laser-welded module is less than or equal to 200 μm [34]. Additionally, the presence of busbars in the air gap could improve the thermal conductance of the air gap, an effect that was not considered here.

In summary, the temperature of a laser-welded module is expected to be within 2 °C of the temperature of conventional modules, resulting in a thermal benefit if the wire diameter and gas cavity thickness can be reduced below about 100 μm. The thermal benefit seen with the thinnest air gaps relates to a 0.6 °C change in annual irradiance-weighted temperatures, which is expected to lower the LCOE by an amount equivalent to that of a 0.1%–0.2% increase in absolute standard temperature conditions (STC) efficiency because of the dependence of operating efficiency and module lifespan on temperature [35]. Furthermore, the thermal benefits of a laser-welded module would become greater for cells with lower optical heat generation (such as passivated emitter and rear totally diffused cells (PERT)

cells), thus offering a pathway to advanced heat mitigation in photovoltaics.

VI. CONCLUSION

This work showed by experimentation and modeling that a polymer-free, glass/glass fs laser-welded module will pass the IEC 61215 static load test at a test load of 5400 Pa. The module design requires embossed indentations and ribs in the glass to allow cells and interconnects to be routed properly and to increase the stiffness of the module, respectively. These preliminary results are promising for a revolutionary change in module design that provides hermetic edge sealing and polymer-free construction to reduce degradation modes, operation temperature, cost, and straightforward recycling by simply breaking the glass to remove the cells and the metal interconnects.

ACKNOWLEDGMENT

The authors would like to thank A. Mitchell and A. Bisson for useful discussions concerning rolled glass properties. The views expressed in the article do not necessarily represent the views of the DOE or the U.S. Government. The U.S. Government retains and the publisher, by accepting the article for publication, acknowledges that the U.S. Government retains a nonexclusive, paid-up, irrevocable, worldwide license to publish or reproduce the published form of this work, or allow others to do so, for the U.S. Government purposes.

REFERENCES

- [1] H. Tada, P. C. Paris, and G. R. Irwin, *The Stress Analysis of Cracks Handbook*, 3rd ed. New York, NY, USA: ASME Press, 2000.
- [2] M. Aghaei et al., "Review of degradation and failure phenomena in photovoltaic modules," *Renewable Sustain. Energy Rev.*, vol. 159, May 2022, Art. no. 112160, doi: [10.1016/j.rser.2022.112160](https://doi.org/10.1016/j.rser.2022.112160).
- [3] F. Madon et al., "Bifacial NICE modules from high efficiency n-type BiSoN solar cells," *Energy Procedia*, vol. 77, pp. 382–385, 2015.
- [4] K. L. Barth, J. Morgante, W. S. Sampath, and T. M. Shimpi, "Progress towards a non lamination encapsulation technology to improve reliability and reduce costs," in *Proc. IEEE 46th Photovolt. Specialists Conf. Chicago*, 2019, pp. 495–498, doi: [10.1109/PVSC40753.2019.8981243](https://doi.org/10.1109/PVSC40753.2019.8981243).
- [5] M. Likins-White, R. C. Tenent, and Z. Zhai, "Degradation of insulating glass units: Thermal performance, measurements and energy impacts," *Buildings*, vol. 13, no. 2, 2023, Art. no. 551, doi: [10.3390/buildings13020551](https://doi.org/10.3390/buildings13020551).
- [6] A. T. Wolf and L. J. Waters, "Factors governing the life expectancy of dual-sealed insulating glass units," *Construction Building Mater.*, vol. 7, no. 2, pp. 101–107, Jan. 1993, doi: [10.1016/0950-0618\(93\)90039-F](https://doi.org/10.1016/0950-0618(93)90039-F).
- [7] S. Z. Rajiv Dubey et al., "Performance of field-aged PV modules in India: Results from 2016 all India survey of PV module reliability," in *Proc. IEEE 44th Photovolt. Specialist Conf.*, 2017, pp. 3478–3481.
- [8] D. S. V. Poulek, I. S. Persic, and M. Libra, "Towards 50 years lifetime of PV panels laminated with silicone gel technology," *Sol. Energy*, vol. 86, no. 1, pp. 3103–3108, 2012.
- [9] R. Couderc, M. Amara, J. Degoulange, F. Madon, and R. Einhaus, "Encapsulant for glass-glass PV modules for minimum optical losses: Gas or EVA?," *Energy Procedia*, vol. 124, pp. 470–477, 2017.
- [10] H. Kind, E. Gehlen, M. Aden, A. Olowinsky, and A. Gillner, "Laser glass frit sealing for encapsulation of vacuum insulation glasses," *Phys. Procedia*, vol. 56, pp. 673–680, 2014.
- [11] S. Emami, J. Martins, L. Andrade, J. Mendes, and A. Mendes, "Low temperature hermetic laser-assisted glass frit encapsulation of sodalime glass substrates," *Opt. Lasers Eng.*, vol. 96, pp. 107–116, 2017.
- [12] A. De Pablos-Martín, S. Rodríguez-López, and M. J. Pascual, "Processing technologies for sealing glasses and glass-ceramics," *Int. J. Appl. Glass Sci.*, vol. 11, pp. 552–568, 2020, doi: [10.1111/ijag.15107](https://doi.org/10.1111/ijag.15107).
- [13] K. Cvecek, R. Odato, S. Dehmel, I. Miyamoto, and M. Schmidt, "Gap bridging in joining of glass using ultra short laser pulses," *Opt. Exp.*, vol. 23, pp. 5681–5693, 2015, doi: [10.1364/OE.23.005681](https://doi.org/10.1364/OE.23.005681).
- [14] H. Chen, L. Deng, J. Duan, and X. Zeng, "Picosecond laser welding of glasses with a large gap by a rapid oscillating scan," *Opt. Lett.*, vol. 44, no. 10, pp. 2570–2573, 2019, doi: [10.1364/OL.44.002570](https://doi.org/10.1364/OL.44.002570).
- [15] K. Cvecek, S. Dehmel, I. Miyamoto, and M. Schmidt, "A review on glass welding by ultra-short laser pulses," *Int. J. Extreme Manuf.*, vol. 1, 2019, Art. no. 042001.
- [16] I. Miyamoto, K. Cvecek, and M. Schmidt, "Advances of laser welding technology of glass—Science and technology," *J. Laser Micro/Nanoeng.*, vol. 15, no. 2, pp. 63–76, 2020.
- [17] J. P. Benthem and W. T. Koiter, "Asymptotic approximations to crack problems," in *Methods of Analysis and Solutions of Crack Problems*, G. C. Sih, Ed. Dordrecht, The Netherlands: Springer, 1973.
- [18] AZO Materials, "Float glass—Properties and applications," *AZO.com*, Accessed on: Jan. 13, 2023. [Online]. Available: <https://www.azom.com/properties.aspx?ArticleID=89>
- [19] D. Young and T. Silverman, "Personal communication: Discussion on rolled glass properties with a major glass manufacturer," Study.com, Mountain View, CA, USA, 2023.
- [20] B. Lawn, *Fracture of Brittle Solids*, 2nd ed. Cambridge, U.K.: Cambridge Univ. Press, 1993.
- [21] Int. Electrotech. Commission, "IEC 61215-1:2021 terrestrial photovoltaic (PV) modules—Design qualification and type approval—Part 1: Test requirements," Accessed on: 2022. [Online]. Available: <https://webstore.iec.ch/publication/68594>
- [22] H. Chen, J. Duan, Z. Yang, W. Xiong, and L. Deng, "Picosecond laser seal welding of glasses with a large gap," *Opt. Exp.*, vol. 27, no. 21, pp. 30297–30307, Oct. 2019, doi: [10.1364/OE.27.030297](https://doi.org/10.1364/OE.27.030297).
- [23] K. Cvecek, S. Dehmel, I. Miyamoto, and M. Schmidt, "A review on glass welding by ultra-short laser pulses," *Int. J. Extreme Manuf.*, vol. 1, no. 4, Dec. 2019, Art. no. 042001, doi: [10.1088/2631-7990/ab55f6](https://doi.org/10.1088/2631-7990/ab55f6).
- [24] J. Xie, "Laser hermetic welding of implantable medical devices," in *Joining and Assembly of Medical Materials and Devices*, Y. Zhou and M. D. Breyer, Eds. Cambridge, U.K.: Woodhead Publishing, 2013, pp. 211–235.
- [25] "Mindrum precision—Materials," Accessed on: Sep. 23, 2023. [Online]. Available: <https://www.mindrum.com/metal/>
- [26] M. Newport, "Bayard-Alpert glass vacuum gauge," Accessed on: Sep. 23, 2023. [Online]. Available: <https://www.newport.com/p/274008>
- [27] Precitec, "Process monitoring for series production," 2015. [Online]. Available: <https://www.precitec.com/laser-welding/products/process-monitoring/>
- [28] Xinology.com, "Solar module lamination and inspection," 2017. [Online]. Available: <http://www.xinology.com/Glass-Processing-Equipments-Supplies-Consumables/glass-photovoltaic/solar-module-production-line/features-specs/solar-module-laminating-inspection.html>
- [29] K. L. Barth, J. Morgante, W. S. Sampath, and T. M. Shimpi, "Progress towards a non-lamination encapsulation technology to improve reliability and reduce costs," in *Proc. IEEE 46th Photovolt. Specialists Conf.*, 2019, pp. 495–498, doi: [10.1109/PVSC40753.2019.8981243](https://doi.org/10.1109/PVSC40753.2019.8981243).
- [30] M. R. Vogt, "Development of physical models for the simulation of optical properties of solar cell modules," Ph.D. dissertation, Leibniz Univ. Hannover, Hannover, Germany, 2015.
- [31] I. Subedi, T. J. Silverman, M. G. Deceglie, and N. J. Podraza, "PERC silicon PV infrared to ultraviolet optical model," *Sol. Energy Mater. Sol. Cells*, vol. 215, Sep. 2020, Art. no. 110655, doi: [10.1016/j.solmat.2020.110655](https://doi.org/10.1016/j.solmat.2020.110655).
- [32] N. P. Irvin et al., "Thermal impact of rear insulation, light trapping, and parasitic absorption in solar modules," *IEEE J. Photovolt.*, vol. 12, no. 4, pp. 1043–1050, Jul. 2022, doi: [10.1109/JPHOTOV.2022.3173785](https://doi.org/10.1109/JPHOTOV.2022.3173785).
- [33] M. Hammami, S. Torretti, F. Grimaccia, and G. Grandi, "Thermal and performance analysis of a photovoltaic module with an integrated energy storage system," *Appl. Sci.*, vol. 7, no. 11, 2017, Art. no. 1107, doi: [10.3390/app7111107](https://doi.org/10.3390/app7111107).
- [34] H. Han, Y. Wu, and C. Ma, "Optimization design of a multibusbar structure: The using of a conductive belt," *Int. J. Photoenergy*, vol. 2018, Jul. 2018, Art. no. 7630390, doi: [10.1155/2018/7630390](https://doi.org/10.1155/2018/7630390).
- [35] L. Xu et al., "Heat generation and mitigation in silicon solar cells and modules," *Joule*, vol. 5, no. 3, pp. 631–645, Mar. 2021, doi: [10.1016/j.joule.2021.01.012](https://doi.org/10.1016/j.joule.2021.01.012).